JOURNAL OF GEOPHYSICAL RESEARCH, VOL. 112, E08S09, doi:10.1029/2006JE002811, 2007

Geologic and spectral mapping of etched terrain deposits in northern Meridiani Planum

J. L. Griffes,[1,2] R. E. Arvidson,[1] F. Poulet,[3] and A. Gendrin[3,4]

Received 11 August 2006; revised 12 January 2007; accepted 30 March 2007; published 3 July 2007.

[1] A ~1 km vertical section of etched terrain and hematite-bearing plains materials and nearby cratered terrain surfaces was mapped in the northern portion of Meridiani Planum using MOC, THEMIS, MOLA, and OMEGA data. The oldest materials are the cratered plains, which have 0.4 to 2.5 μm spectral reflectance dominated by a mix of low and high calcium pyroxenes. Etched plains materials overlie this unit and are exposed within a 120 km NW-SE trending valley to the south of the cratered plains. Lower etched plains materials exhibit a kieserite signature on a plateau-forming horizon and polyhydrated sulfate signatures on the main valley floor. The upper etched plains unit exhibits signatures consistent with hydrated iron oxides and is covered by what is interpreted to be a relatively thin layer of basaltic sand and hematitic concretions (the hematite-bearing plains unit). The youngest unit consists of ejecta deposits from a cluster of six craters that mantle the eastern portion of the study area. The thick section of etched plains materials (~900 m) with exposures of hydrated sulfates and hydrated iron oxides implies that measurements made by the Opportunity rover (located ~390 km to the southwest of the study area) are at the top of an extensive section of layered sedimentary materials formed in and/or altered in an aqueous environment and exposed by aeolian erosion.

Citation: Griffes, J. L., R. E. Arvidson, F. Poulet, and A. Gendrin (2007), Geologic and spectral mapping of etched terrain deposits in northern Meridiani Planum, *J. Geophys. Res.*, *112*, E08S09, doi:10.1029/2006JE002811.

1. Introduction

[2] The purpose of this paper is to present and analyze geomorphic, stratigraphic, and mineralogical information for a series of five units identified and mapped in northern Meridiani Planum (Figure 1). Mars Global Surveyor Mars Orbiter Camera (MOC) [*Malin et al.*, 1992] and Mars Orbiter Laser Altimeter (MOLA) [*Smith et al.*, 2001], Mars Odyssey Thermal Emission Imaging System (THEMIS) [*Christensen et al.*, 2004], and Mars Express Observatoire pour la Minéralogie, l'Eau, les Glaces et l'Activité (OMEGA) [*Bibring et al.*, 2005] data were jointly analyzed for a region extending from −2.25°E to 1°E and 0.25°N to 4°N. The study area includes the hematite-bearing plains mapped from orbit by the Mars Global Surveyor Thermal Emission Spectrometer (TES) [*Christensen et al.*, 2000], the underlying etched terrain materials [*Hynek et al.*, 2002; *Arvidson et al.*, 2003], and sulfate exposures mapped by OMEGA [*Gendrin et al.*, 2005; *Arvidson et al.*, 2005] as well as exposures of densely cratered terrain. This specific study site was chosen because of the rich diversity of distinct units exposed in a relatively small area and because of the ~1 km of stratigraphic section exposed, thereby providing the opportunity to study these regions in detail (Figures 1 and 2).

2. Morphologic and Stratigraphic Mapping

[3] The study area is located in Meridiani Planum where four major geologic units had been mapped prior to acquisition of THEMIS or OMEGA data [*Hynek et al.*, 2002; *Arvidson et al.*, 2003] (Figure 1). The base of the regional-scale stratigraphic section consists of dissected cratered terrain (DCT), a unit characterized by low albedo, densely cratered surfaces that are dissected by valley networks. Several hundred meters of the etched terrain (E) layered deposits unconformably overlie the DCT unit. The E unit has a higher albedo and thermal inertia compared to cratered terrains and exhibits various erosional features such as mesas, pits, ridges and polygonal terrain interpreted to have formed by differential aeolian erosion of layered deposits [*Arvidson et al.*, 2003; *Edgett*, 2005]. The next youngest unit is the hematite-bearing plains (Ph), which is dark, smooth and laterally extensive. *Christensen et al.* [2000] used Thermal Emission Spectrometer (TES) data to infer the presence of coarse-grained crystalline hematite. Detailed examination of the Ph surfaces by the Opportunity rover, coupled with analyses of OMEGA data, show that the Ph unit surface materials are an aeolian deposit of poorly sorted

[1]Department of Earth and Planetary Sciences, Washington University, St. Louis, Missouri, USA.
[2]Center for Earth and Planetary Studies, National Air and Space Museum, Smithsonian Institution, Washington, D. C., USA.
[3]Institut d'Astrophysique Spatiale, Université Paris-Sud, Orsay, France.
[4]Department of Geological Sciences, Brown University, Providence, Rhode Island, USA.

0148-0227/07/2006JE002811$09.00

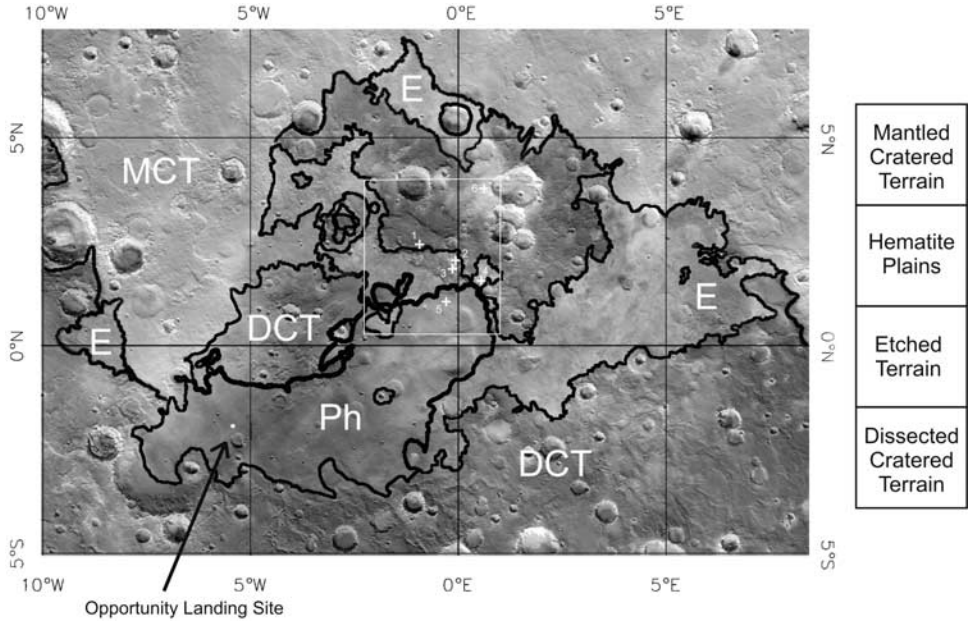

Figure 1. MOC wide-angle image mosaic derived from Geodesy Campaign data [*Caplinger and Malin*, 2001] overlain by regional geologic map units for Meridiani Planum: Dissected Cratered Terrain (DCT), Etched Terrain (E), Hematite-Bearing Plains (Ph), and the Mantled Cratered Terrain (MCT) (stratigraphic column shown at right). Units from *Arvidson et al.* [2003]. Opportunity landing site shown as white dot. Area analyzed in detail for this paper is outlined as white box. Note the cluster of six craters located on the northeastern portion of the study area. Spectral end-members derived from OMEGA data for the study area are shown as Cratered Plains (1, CP), Lower and Upper Etched Plains (2, 3 LEP and 4, UEP), Hematite-Bearing Plains (5, Ph), and Dust (6).

basaltic sand and a lag deposit of hematitic concretions. These materials overlie sulfate-rich rocks (presumably the top of the E unit) [*Squyres et al.*, 2004; R. E. Arvidson et al., Coordinated analysis of Mars Express OMEGA and Mars Exploration Rover traverse data for Meridiani Planum, submitted to *Journal of Geophysical Research*, 2006 (hereinafter referred to as Arvidson et al., submitted manuscript, 2006)]. To the north of the study site, the DCT and other units have been mantled and comprise the Mantled Cratered Terrain (MCT) unit.

[4] The current study focuses on a much more detailed mapping and analysis of units as compared to previous analyses. The region is located ~390 km to the northeast of the Opportunity landing site and is centered on a 120-km-long northwest-southeast trending valley with ~1 km of relief. Our approach was to first define geologic units on the basis of morphology, superposition, and embayment relationships using THEMIS, MOC, and MOLA data. The base map for the work consisted of the 128 pixel/degree gridded MOLA elevation data. In addition, this study also incorporated full resolution MOLA along track estimates of elevation (~300 m MOLA shot-to-shot) for several regions for which MOC Narrow Angle (NA) images were also acquired (Table 1). THEMIS images used in this study include daytime and nighttime IR scaled brightness products [*Christensen et al.*, 2004]. Daytime IR images were used because differential solar heating emphasizes topographic features at the late afternoon times of observation (~17:00 Local True Solar Time (LTST) equatorial crossing time), although albedo and thermal inertia effects are also evident. Nighttime IR data, acquired predawn (equatorial crossing time ~05:00 LTST), were also included because brightness values are controlled by thermal inertia [*Christensen et al.*, 2001]. That is, the residual thermal effect of the differential solar heating due to topography and albedo variations have largely dissipated by the predawn observation time for nighttime THEMIS observations. Estimates of terrain roughness averaged over ~75 m scales were derived from MOLA intrashot pulse spread estimates, and RMS heights over ~300 m spatial wavelengths were determined by MOLA along track shot to shot measurements. Finally, Lambert albedo and thermal inertia (TI) values for the units mapped as part of this study were extracted from TES-based products presented by *Arvidson et al.* [2003] and *Mellon et al.* [2001]. Table 1 summarizes the data sets used in the study, and Table 2 summarizes characteristics of each unit.

[5] On the basis of detailed examination of the THEMIS, MOLA, and MOC data discussed above, five geologic units were mapped in the study area (Figures 2–4 and Table 2). The base of the stratigraphic column is the cratered plains (CP) unit, characterized by relatively smooth, low albedo plains with intermediate thermal inertia values (Table 2). Elevation data show that the CP unit is located on a set of northwest-southeast trending ridges and intervening valleys. To the east it is covered by the youngest unit, i.e., ejecta deposits (cratered terrain, CT) from the cluster of six craters located on the northeastern boundary of the study area (Figure 1). This unit is equivalent to unit DCT on the

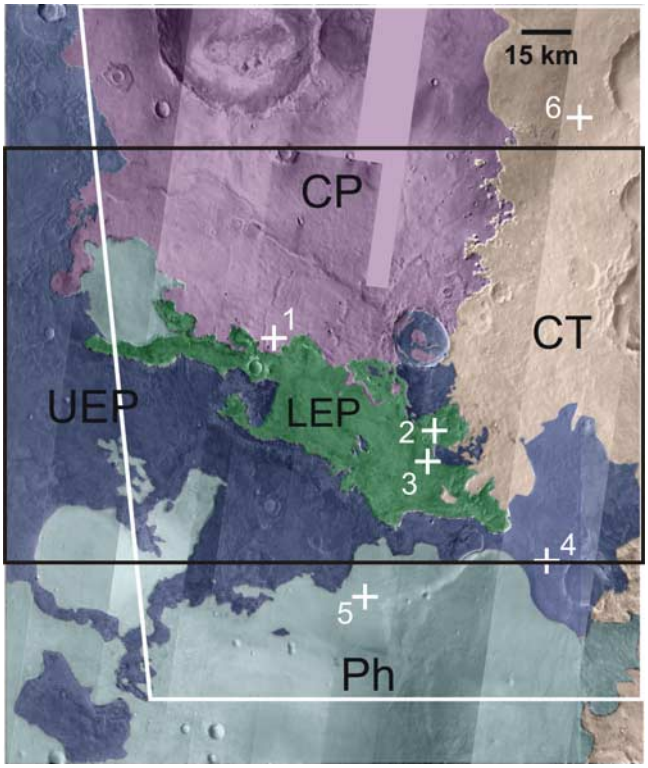

Figure 2. THEMIS daytime infrared image mosaic overlain by geologic units defined in this study. Oldest unit is CP, followed by LEP and UEP, and Ph, and the youngest is the CT unit. White box shows footprint for OMEGA Orbit 485, and black box shows location for enlarged versions of THEMIS mosaics depicted in Figures 4 and 5. Numbers refer to spectral end-member locations for OMEGA data.

regional map (Figure 1). To the south, the CP unit is covered by the lower etched plains (LEP) materials. The superposition relationships for the transition to the CT unit are evident in the elevation data, which show a ragged cliff (~250 m high) bounding the eastern edge of the CP unit (Figure 3). The cliff is also evident in the daytime IR and is clearly shown in the nighttime IR to be associated with partially eroded ejecta deposits from the group of six craters located to the northeast of the detailed study area (Figures 1–5). Other superposition relationships are also evident in the IR data. In particular, a trough or channel can be seen in the daytime IR data in the CP unit that extends from a ridge to the southwest and disappears beneath the LEP unit (Figure 4).

[6] LEP materials occupy the lowest portions of the 120-km-long northwest-southeast trending valley and are characterized by relatively medium albedos and modestly high thermal inertias (Table 2). The valley forming portion of this unit is ~150 meters thick based on elevation data from MOC NA image M21-00093 and its corresponding MOLA track, which was taken near the northwest contact of the LEP and CP units. The upper portion of the LEP unit is exposed on a plateau on the northeastern side of the valley. The LEP materials partially cover ejecta deposits from a 20-km-wide crater on the CP unit. The CT ejecta deposits also partially cover the ejecta from this 20-km-wide crater. The LEP unit is characterized by a wide variety of landforms suggestive of differential wind erosion of indurated layered materials. These include smooth plains, groups of mesas and mounds, and dune fields. This unit has the highest MOLA intrashot roughness and shot-shot RMS height of any of the units. It is also the location where *Gendrin et al.* [2005] and *Arvidson et al.* [2005] in a reconnaissance study found evidence for kieserite and polyhydrated sulfates using OMEGA data sets.

[7] The upper etched plains (UEP) unit (~250 m thick based on corresponding MOLA track to MOC NA image E01-02092) is a plateau-forming unit that is topographically and stratigraphically higher than the LEP unit and surrounds the valley to the south and east. The south of the UEP unit is covered by the hematite-bearing plains (Ph) unit (Figures 2–5). The UEP is characterized by medium albedos and the highest thermal inertias within the study area. This unit exhibits a geomorphic pattern that ranges from relatively flat plains to dissected plateaus that exhibit fine-scale layering. The Ph unit is extensively exposed in the southern portion of the study area and appears dark and smooth in high resolution MOC NA images, with patches of dune fields. The Ph unit, based on observations by Opportunity, is interpreted to be a thin (~1 m) aeolian mantle of basalt sand and hematitic concretions sitting on the UEP unit.

Table 1. Summary of Data Used in the Study[a]

Data Set	Frames	Characteristics
OMEGA	Orbits 485-2 and 485-3	LTST: ~9:00 LST Pixel size: ~2 km Incidence angle: 46 deg
THEMIS Daytime IR	I10323014, I09387010, I01735006, I01373009, I09674020, I09362003, I02434005, I03520002, I03907004, I11496006	100 m/pixel acquired ~17:00 LST
THEMIS Nighttime IR	I07509009, I07147010, I07896011, I06373008, I07871013, I07484005, I07846015, I01879002, I07459005, I06710010, I05599012, I09481002	100 m/pixel acquired ~5:00 LST
MOC NA frames and associated MOLA elevation tracks	E0500328 (MOLA pass #20014) E0500329 M0204582 (MOLA pass #11376) E10-04085	~14:00–15:00 LST Pixel size range: 4.35–5.86 m/pixel

[a]Values for OMEGA data are for the location of the kieserite signature in the lower etched plains.

Table 2. Mapped Unit Descriptions and Characteristics[a]

Geologic Unit	Geomorphic Characteristics	Ancillary Properties	OMEGA-Based Mineralogical Inferences
CT: ejecta deposits from six craters	ejecta deposits	Albedo: 0.24[b] TI: 246 ± 12 PW: ~1 Alt: 1683 ± 72	nanophase iron oxides where dust-covered in north and pyroxene dominated sands in south
Ph: hematite-bearing plains	smooth plains with occasional dunes and exposure of brighter plains	Albedo: 0.15 TI: 184 ± 17 PW: ~1 Alt: 1790 ± 124	hematitic concretions and basaltic sand over etched terrain materials
UEP: upper etched plains	plateau-forming plains with scalloped appearance, occasional dunes and mesas	Albedo: 0.25 TI: 373 ± 46 PW: 1.4 ± 0.6 Alt: 1664 ± 97	hydrated iron oxides
LEP: lower etched plains	complex of dunes, mounds, mesas, smooth plains	Albedo: 0.17 TI: 325 ± 28 PW: 2 ± 1 Alt: 1596 ± 97	polyhydrated sulfates with horizon exposing kieserite
CP: cratered plains	dark relatively smooth plains with ridges and channel systems	Albedo: 0.12 TI: 245 ± 10 PW: ~1 Alt:1621 ± 111 (ridge)	basaltic sands with a mix of low and high calcium pyroxenes

[a]Albedo is based on 1.3 μm I/F/cosine(i) from OMEGA 485 data, where I is the radiance sensed by OMEGA, *F* is the solar irradiance/Π and i is the solar incidence angle. Thermal inertia (TI) from *Arvidson et al.* [2003] in SI units. MOLA intrashot pulse width in meters from *Neumann et al.* [2001] and MOLA gradient based on 128 pixel/degree gridded data. Alt is altitude in meters referenced to the MOLA-based areoid [*Zuber et al.*, 1992].
[b]For CT unit, the albedo and TI values correspond to the bright dusty surfaces. The lower albedo CT exposures have values similar to the CP unit.

[8] Finally, the uppermost unit consists of ejecta deposits associated with the CT unit (~250 m thick based on the elevation difference between the CP unit and the CT unit to the east), which is well exposed in the eastern-most portion of the study area. This unit has a variable albedo and TI signature ranging from dust-like values in the north to values similar to those for the CP unit in the southern portion of the study area (e.g., Figure 1 and Table 2).

3. Spectral Reflectance Characteristics and Mapping

[9] The focus of the OMEGA-based part of this study is the data from the C Spectrometer (128 bands in the wavelength range of 0.93 to 2.73 μm) because this system is well-calibrated, free from competing effects of solar radiation and thermal emission found at longer wavelengths, and is the wavelength range that is rich in information about iron-bearing silicates, hydrated phases, and hydroxylated phases. Data utilized are from OMEGA orbit 485 acquired at approximately 9 AM Mars LTST at a solar incidence angle of 46 degrees (Table 1). OMEGA data are presented as retrieved surface reflectances (I/F which is atmosphere-free surface radiance at the sensor divided by the solar irradiance at the top of the Martian atmosphere divided by π). The retrievals were obtained as described by *Bibring et al.* [2005], in which gas bands were removed by normalizing to the ratio of spectra acquired from the top of Olympus Mons compared to the surrounding plains. Aerosols have not been removed but do not greatly influence mapping of minerals for the C Spectrometer (Arvidson et al., submitted manuscript, 2006).

[10] Figure 6 shows a false color image (with a linear 2% stretch) of OMEGA orbit 485 with red at 2.2722 μm, green at 1.5004 μm, and blue at 1.1411 μm. This wavelength combination was found, by inspection, to optimally show false color variations associated with the surface. The CP unit is dark and gray in the composite, whereas the LEP unit

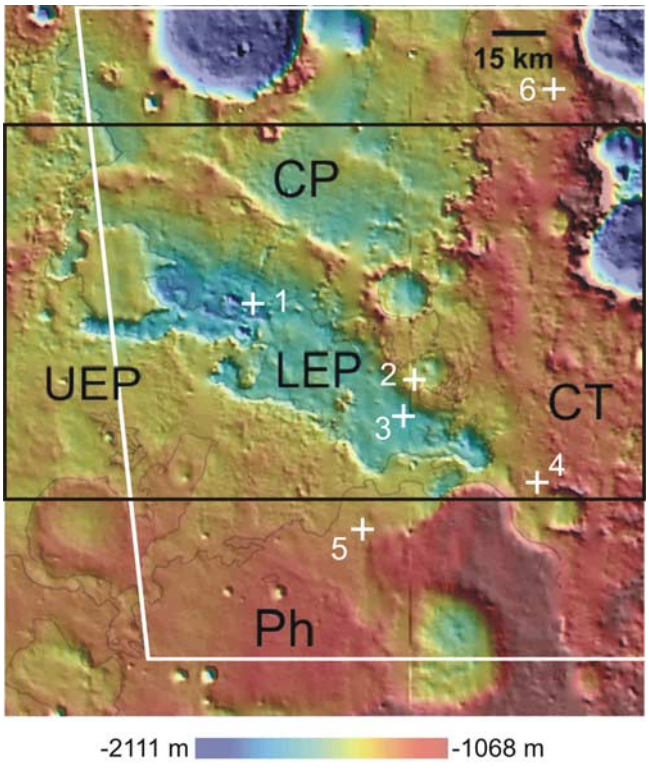

Figure 3. MOLA shaded relief map overlain by color-coded topography for study area. Box, units, and numbering scheme defined in Figure 2. The CP unit is located on plains with a northwest-southeast trending ridge. Note that the LEP unit is located in a northwest-southeast trending valley to the southwest of the CP unit. UEP is a plateau-forming unit that is topographically above the LEP, and the Ph unit lies topographically above the UEP. Note dissected boundary of CT unit. Section thickness is variable but in places is ~900 m. MOLA data are gridded at 128 pixels/degree [see *Smith et al.*, 2001].

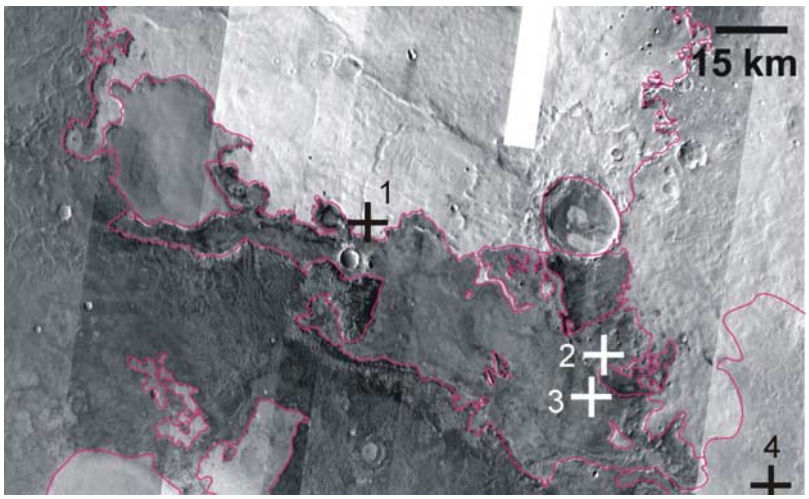

Figure 4. THEMIS daytime scaled brightness infrared image mosaic of the study area. With an acquisition local solar time of ~17:00, differential solar heating allows topographic variations to be discerned and modulated by albedo and thermal inertia properties. Note the plains-like nature of the CP unit and the northwest-southeast trending ridge. Isolated part of Ph unit to the west of the valley shows that these materials are superimposed on the CP unit. LEP are in the northwest-southeast trending valley evident in MOLA data, whereas the UEP are topographically (and stratigraphically) above the LEP. UEP materials range from relatively low to high temperatures in the mosaic. CT located in upper right is seen superimposed on other units. Locations of spectral end-members are shown as numbers. See *Christensen et al.* [2001] for description of THEMIS data sets.

exhibits a range of brown colors and the UEP is bright and fairly homogeneous. The Ph unit is variable, but with a relatively low brightness and brown color. The CT unit in the northeastern part of the study area is bright and in the southeastern part it is dark and gray. The minimum noise fraction principal component rotation [*Boardman and Kruse*, 1994] was used to further refine the patterns in the C Spectrometer data and to search for end-members and the extent to which they correspond to geologic units mapped from geomorphologic and elevation patterns. Factor loadings onto the first component are dominated by overall brightness of the spectra. The second two factors account for 12% of the variance associated with the 128 band data set (with bad pixels first removed). These two factor

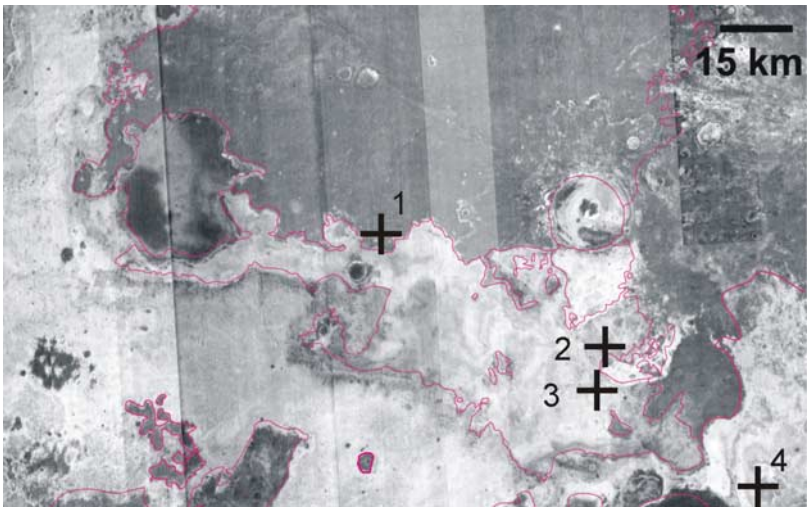

Figure 5. THEMIS nighttime infrared scaled brightness image mosaic acquired ~5:00 local solar time. Thermal inertia controls brightness at this time since differential solar heating due to albedo and topographic variations is subdued after nighttime cooling takes place. Note the relatively cool temperatures of the CP and Ph units as compared to the warmer (i.e., higher thermal inertia) etched units. See Table 2 for detailed albedo and TES-based thermal inertia values for all mapped units.

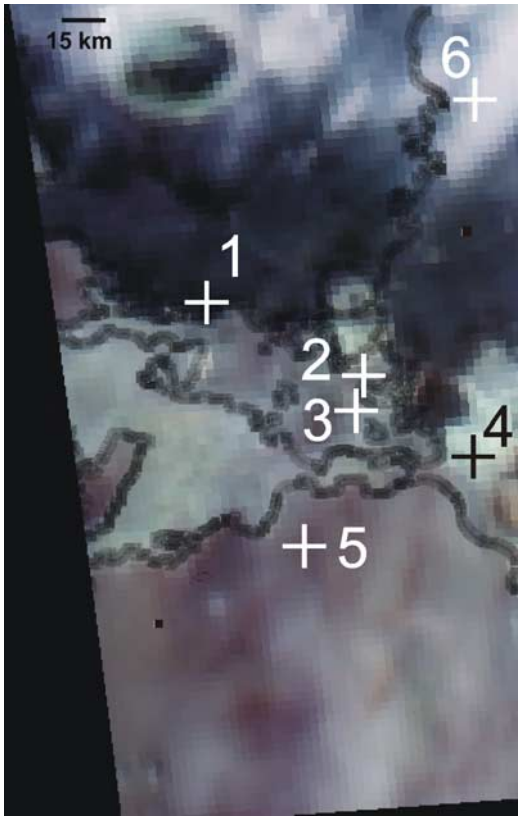

Figure 6. OMEGA Orbit 485 false color image (R: 2.2733 μm, G: 1.5004 μm, B: 1.1411 μm). The CP unit is dark and relatively gray, Ph is variable in albedo and red, and the LEP unit is relatively dark as compared to the UEP. Bright dust deposits can be seen in the top of the image. CT shows variable color, from the bright dust signature to the dark, relatively gray signature characteristic of the CP unit. Spectral end-member locations are shown.

loadings are shown as a scatterplot in Figure 7 and clearly show that the extent to which end-members are associated with the factor loadings. Spectral end-members were isolated as the individual extreme pixel for each lobe in the MNF scatterplot.

[11] In fact, end-member locations associated with the principal component rotations are within the geologic units mapped on the basis of geomorphic and elevation data sets, with the exception of the CT unit (Figures 2–6). For reference, the end-member spectra are shown in Figure 8 and locations are given in preceding figures. The dust spectrum is located in the northern part of the CT unit and is typical of spectra for bright areas on Mars. It has been shown to be best modeled as due to the presence of anhydrous palagonitic-like dust in which ferric charge transfer and electronic transition absorptions dominate [*Morris et al.*, 2001; *Bibring et al.*, 2005]. The CT unit is partly characterized by the dust end-member and partly by the CP end-member. The CP end-member spectrum is clearly dominated by pyroxene bands at $\sim$1 and $\sim$2 μm (Figure 8). Specifically, low calcium pyroxenes (LCP) have band centers at 0.9 μm and 1.8 μm, whereas high calcium pyroxenes (HCP) have band centers at 1.05 μm and 2.3 μm [*Pieters et al.*, 1996, *Mustard et al.*, 2005]. We have pursued use of the modified Gaussian method (i.e., MGM, which models the continuum-removed spectrum as a suite of Gaussian functions with varying width, centers, and amplitudes) to identify and map LCP and HCP band depths and centers [*Sunshine and Pieters*, 1993; *Pieters et al.*, 1996; *Sunshine et al.*, 1990]. Results show that the CP unit contains spectral evidence for both LCP (i.e., the band depth centered at 1.9 μm) and HCP (2.3 μm) (Figures 9 and 10) [*Gendrin et al.*, 2006]. MGM results also show that LCP dominates the HCP band depth. This is unusual for Mars and is exhibited in OMEGA data only on older cratered plains [*Mustard et al.*, 2005].

[12] The spectra associated with Ph, UEP, and LEP units deserve detailed analysis. Arvidson et al. (submitted manuscript, 2006) show that the relatively flat spectra acquired over the Ph unit at the Opportunity landing site can be modeled by a mixture of hematite, plagioclase, pyroxene and dust. Similarities to the Ph spectrum over Opportunity argue for a similar interpretation for the Ph unit in the current study site. The UEP unit end-member spectrum exhibits a 1.92 μm feature due to the $\nu_2 + \nu_3$ combination vibration associated with molecular water [*Arvidson et al.*, 2005]. The steep slope at shorter wavelengths is consistent with an enhanced abundance of ferric oxides relative to other units. There is a 2.4 μm feature although the broad nature of this dip precludes identification of the vibrational mode or modes, e.g., whether or not it is related to vibrational modes of water in sulfate lattices. There is also

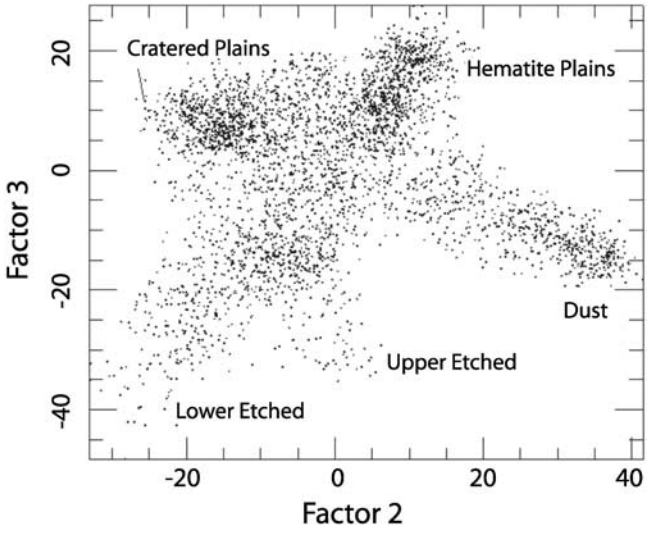

Figure 7. Scatterplot showing the factor loadings for factors 2 and 3 for a minimum noise fraction coordinate rotation for OMEGA Orbit 485 C Spectrometer data (1 to 2.7 μm) for the study area. Locations of end-member spectra identified in the rotation are shown and correspond to CP, LEP, UEP, and Ph units, and northern exposures of the CT (dust). There is a good correspondence between geologic units based on geomorphology and spectral properties, with the exception that CT ranges from dust to CP signatures.

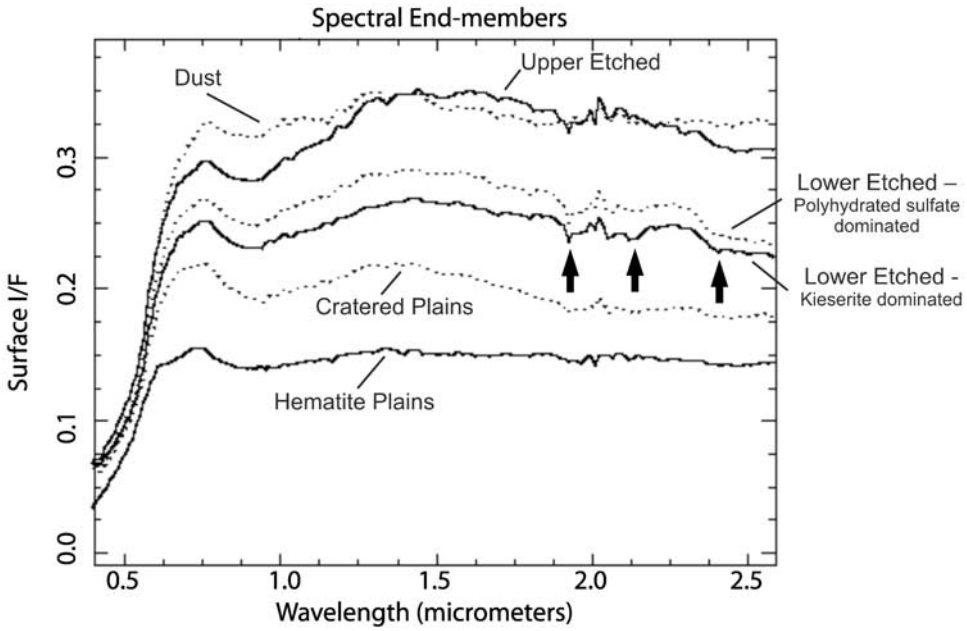

Figure 8. VNIR and C spectrometer spectra for the end-members shown in Figure 7. The CP spectrum shows absorption features at ~1 and ~2 μm, consistent with the spectral dominance by pyroxene. The Ph spectrum is relatively flat, whereas the LEP spectrum shows absorption features at 1.92, 2.1, and 2.4 μm (see arrows). The UEP spectrum is brighter, has a higher 1 to 1.4 μm slope, and exhibits a 1.92 μm absorption only, relative to the LEP unit.

an indication of a shallow 2.3 μm band, although the reality of this band is called into question by the fact that the depth is within the uncertainty envelope associated with instrument non-linearities. We thus do not pursue analysis of this band further.

[13] The LEP end-member spectra (Figure 8) based on the 2.1 and 2.4 μm features are strongly suggestive of the presence of water in one or more of the kieserite-family of minerals, where kieserite has the formula $MgSO_4 \bullet H_2O$. This family includes minerals with a formula of $Me(II)SO_4 \bullet H_2O$, where Me = Mn, Fe, Co, Ni, and Zn [*Mildner and Geister*, 1991]. Of particular interest is szomolnokite, the Fe version of the kieserite family. *Arvidson et al.* [2005] conclude that kieserite is the best match, since the other candidates have transition metal cations which have strong electronic absorptions from 0.4 to 1.5 micrometers that are not evident in the data. The LEP end-member spectrum also shows a strong 1.92 μm feature which, combined with the 2.4 μm feature, is diagnostic of polyhydrated sulfates [*Gendrin et al.*, 2005]. Specific band depth estimates for these the 2.1 and 2.4 μm features were generated and mapped as follows:

R = I/F, i.e., surface reflectance

$$\text{Depth } 2.1 = -(2{*}R(2.12) + R(2.15))/(R(1.93) + R(1.94) + R(1.96) + R(2.25) + R(2.26) + R(2.27))$$

$$\text{Depth } 2.4 = 1 - (2{*}R(2.41) + R(2.42))/(R(2.30) + 2{*}R(2.31))$$

[14] The 2.1 μm band depth shows high values on the plateau on the eastern portion of the LEP unit, as well as

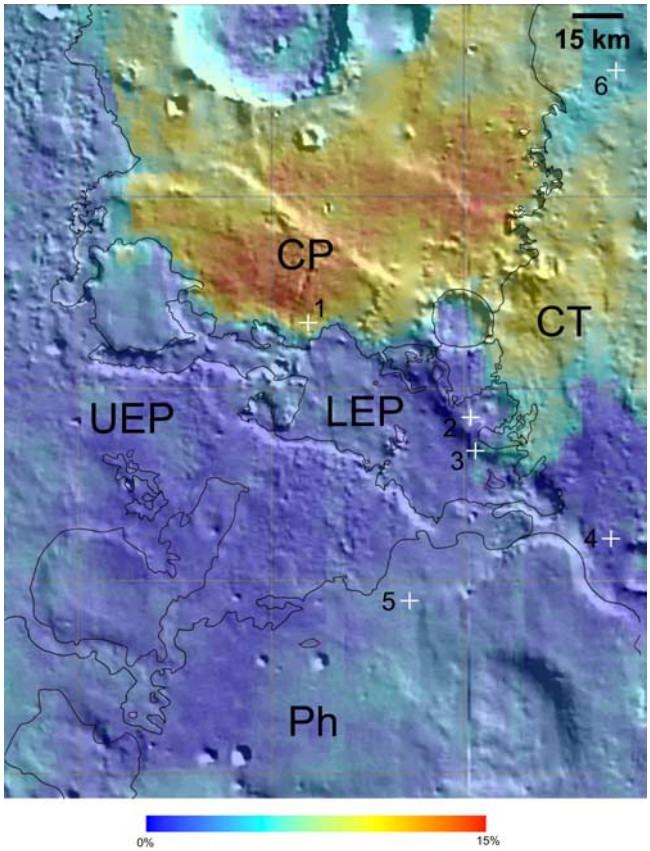

Figure 9. OMEGA MGM results showing Low Calcium Pyroxene (LCP) band depth (from 0% to 15%), overlain on MOLA shaded relief.

along the cliffs of the southern and western portions of the valley (Figure 11). The 2.4 μm band depth map shows high values where the 2.1 μm band depth is lower (Figure 11). These results suggest that the kieserite and polyhydrated phases co-occur but that the polyhydrated phase dominates exposures on the main valley floor. Both band depth maps show that the UEP unit has low values of both 2.1 and 2.4 μm band depths.

4. Summary and Implications

[15] The geomorphology, spectral properties and stratigraphy indicate that a well-defined sequence of units (~1 km thick) was deposited unconformably over cratered plains in the area studied in northern Meridiani Planum. Erosion has since exposed these materials. The Cratered Plains are an intercrater plains unit and are dominated by low and high calcium pyroxenes (LCP and HCP). These are interpreted to be old flows on Noachian cratered terrains. A sedimentary origin seems most likely for the layered deposits found in Meridiani due to the presence of hydrated sulfates since these materials form in the presence of liquid water as an evaporite and/or via groundwater diagenesis. The differences in mineralogy and hydration found for the lower as opposed to the upper etched plains imply that the aqueous conditions varied during emplacement and/or alteration of the ~900 m layered materials. Finally, the outcrops explored by Opportunity (located ~390 km to the southwest of the study site) are interpreted to be the uppermost layer of etched terrain materials similar in nature to the Upper Etched Plains materials.

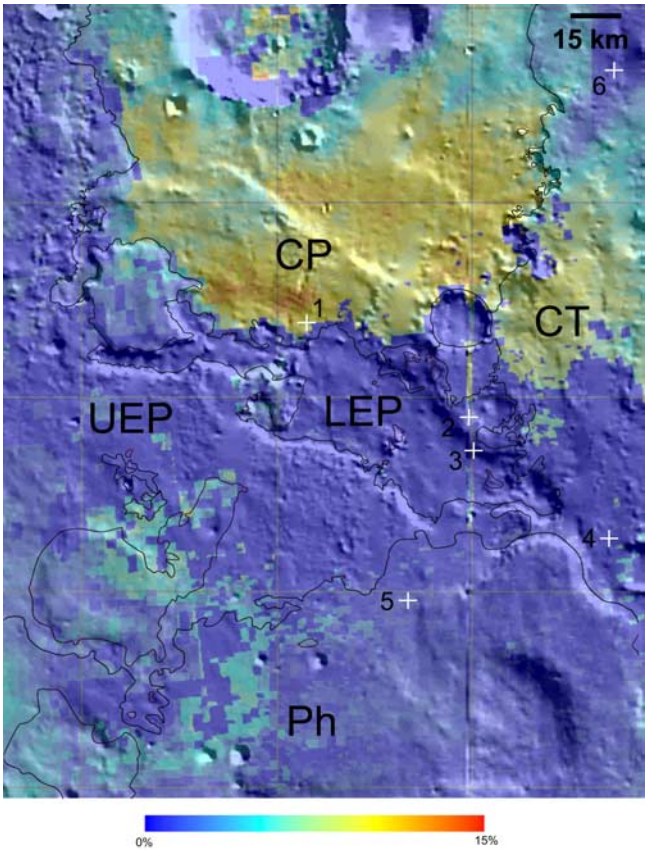

Figure 10. OMEGA MGM results showing High Calcium Pyroxene (HCP) band depth (from 0% to 15%), overlain on MOLA shaded relief.

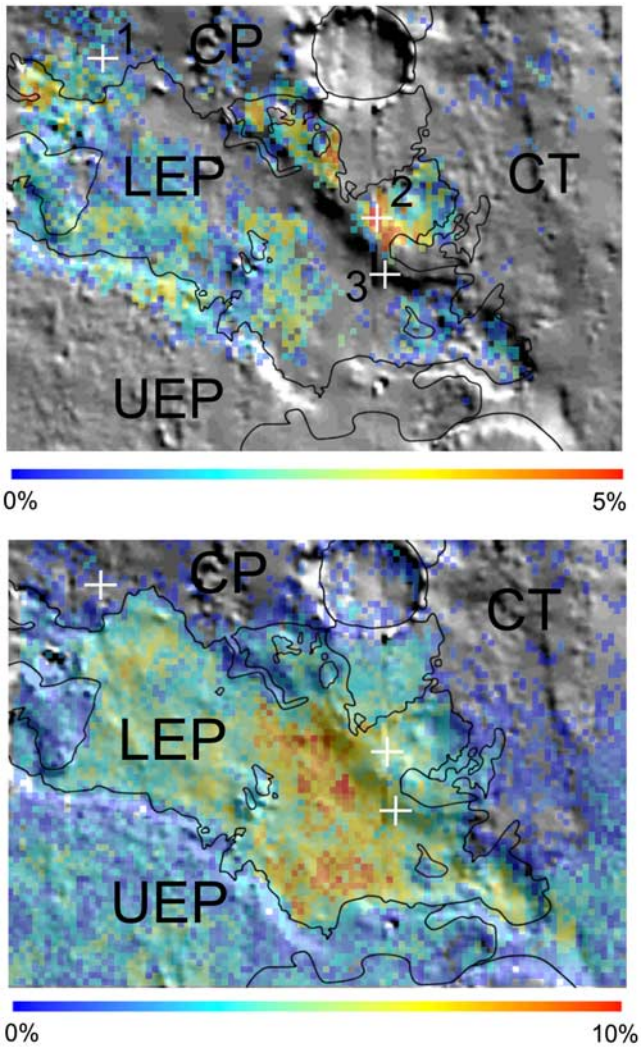

Figure 11. (top) The 2.1 μm band depth from OMEGA overlain on MOLA shaded relief showing abundance of what is interpreted to be kieserite, which has a distinct 2.1 μm feature. Strongest signature appears in the plateau area to the northeast of the valley, and along the valley edges. (bottom) The 2.4 μm band depth from OMEGA overlain on MOLA shaded relief showing abundance of polyhydrated sulfates. Strongest signature runs along the valley floor, where the 2.1 μm kieserite signature is not as evident. Color bars represent strength of band depth.

[16] **Acknowledgments.** J.G. was supported by the NASA Planetary Geology and Geophysics Program from the NASA Goddard Space Flight Center. R.A. was supported by the same grant, in addition to a contract from the Jet Propulsion Laboratory to participate on the OMEGA Team as a Liaison Member from the CRISM Team. A.G. was supported by Marie-Curie OIF Fellowship 8579.

References

Arvidson, R. E., F. P. Seelos IV, K. S. Deal, W. C. Koeppen, N. O. Snider, J. M. Kieniewicz, B. M. Hynek, M. T. Mellon, and J. B. Garvin (2003), Mantled and exhumed terrains in Terra Meridiani, Mars, *J. Geophys. Res.*, *108*(E12), 8073, doi:10.1029/2002JE001982.

Arvidson, R. E., F. Poulet, J.-P. Bibring, M. Wolff, A. Gendrin, R. V. Morris, J. J. Freeman, Y. Langevin, N. Mangold, and G. Bellucci (2005), Spectral reflectance and morphologic correlations in eastern Terra Meridiani, Mars, *Science*, *307*, 1591–1594, doi:10.1126/science.1109509.

Bibring, J.-P., et al. (2005), Mars surface diversity as revea0led by the OMEGA/Mars Express observations, *Science*, *307*, 1576–1581, doi:10.1126/science.1109509.

Boardman, J. W., and F. A. Kruse (1994), Automated spectral analysis: A geologic example using AVIRIS data, north Grapevine Mountains, Nevada, in *Proceedings, 10th Thematic Conference on Geologic Remote Sensing*, pp. 407–418, Environ. Res. Inst. of Mich., Ann Arbor.

Caplinger, M. A., and M. C. Malin (2001), Mars Orbiter Camera geodesy campaign, *J. Geophys. Res.*, *106*, 23,595–23,606.

Christensen, P. R., et al. (2000), Detection of crystalline hematite mineralization on Mars by the Thermal Emission Spectrometer: Evidence for near-surface water, *J. Geophys. Res.*, *105*, 9623–9642.

Christensen, P. R., et al. (2001), Mars Global Surveyor Thermal Emission Spectrometer experiment: Investigation description and surface science results, *J. Geophys. Res.*, *106*, 22,823–22,871.

Christensen, P. R., et al. (2004), The Thermal Emission Imaging System (THEMIS) for the Mars 2001 Odyssey Mission, *Space Sci. Rev.*, *110*, 85–130.

Edgett, K. (2005), The sedimentary rocks of Sinus Meridiani: Five key observations from data acquired by the Mars Global Surveyor and Mars Odyssey orbiters, *Mars J.*, *1*, 5–58, doi:10.1555/mars.2005.0002.

Gendrin, A., et al. (2005), Sulfates in Martian layered terrains: The OMEGA/Mars Express view, *Science*, *307*, 1587–1591, doi:10.1126/science.1109509.

Gendrin, A., et al. (2006), Strong pyroxene absorption bands on Mars identified by OMEGA: Geological counterpart, *Lunar Planet. Sci.*, *XXXVII*, Abstract 1858.

Hynek, B. M., R. E. Arvidson, and R. J. Phillips (2002), Geologic setting and origin of Terra Meridiani hematite deposit on Mars, *J. Geophys. Res.*, *107*(E10), 5088, doi:10.1029/2002JE001891.

Malin, M. C., G. E. Danielson, A. P. Ingersoll, H. Masursky, J. Veverka, M. A. Ravine, and T. A. Soulanille (1992), Mars Observer Camera, *J. Geophys. Res.*, *97*, 7699–7718.

Mellon, M. T., B. M. Jakosky, H. H. Kieffer, and P. R. Christensen (2001), High-resolution thermal inertia mapping from the Mars Global Surveyor Thermal Emission Spectrometer, *Icarus*, *148*, 255–437.

Mildner, M., and G. Geister (1991), The crystal structures of kieserite-type compounds. 1. Crystal structures of Me (II)SO4 H2O (Me = Mn, Fe, Co, Ni, Zn), *Neues Jahrb. Mineral. Monatsh.*, *7*, 296–306.

Morris, R. V., D. C. Golden, D. W. Ming, T. D. Shelfer, L. C. Jorgensen, J. F. Bell III, T. G. Graff, and S. A. Mertzman (2001), Phyllosilicate-poor palagonitic dust from Mauna Kea volcano (Hawaii): A mineralogical analogue for magnetic Martian dust?, *J. Geophys. Res.*, *106*, 5057–5083.

Mustard, J. F., F. Poulet, A. Gendrin, J.-P. Bibring, Y. Langevin, B. Gondet, N. Mangold, G. Bellucci, and F. Altieri (2005), Olivine and pyroxene diversity in the crust of Mars, *Science*, *307*, 1594–1597, doi:10.1126/science.1109509.

Neumann, G. A., D. D. Rowlands, F. G. Lemoine, D. E. Smith, and M. T. Zuber (2001), The crossover analysis of MOLA altimetric data, *J. Geophys. Res.*, *106*, 23,753–23,768.

Pieters, C. M., J. F. Mustard, and J. M. Sunshine (1996), Quantitative mineral analyses of planetary surfaces using reflectance spectroscopy, in *Mineral Spectroscopy: A Tribute to Roger G. Burns*, edited by M. D. Dyar, C. McCammon, and M. W. Schaefer, *Spec. Publ. Geochem. Soc.*, *5*, 307–325.

Smith, D. E., et al. (2001), Mars Orbiter Laser Altimeter: Experiment summary after the first year of global mapping of Mars, *J. Geophys. Res.*, *106*, 23,689–23,722.

Squyres, S. W., et al. (2004), The Opportunity rover's Athena science investigation at Meridiani Planum, Mars, *Science*, *306*(5702), 1698–1703, doi:10.1126/science.1106171.

Sunshine, J. M., and C. M. Pieters (1993), Estimating modal abundances from the spectra of natural and laboratory pyroxene mixtures using the modified Gaussian model, *J. Geophys. Res.*, *98*, 9075–9087.

Sunshine, J. M., C. M. Pieters, and S. F. Pratt (1990), Deconvolution of mineral absorption bands: An improved approach, *J. Geophys. Res.*, *95*, 6955–6966.

Zuber, M. T., D. E. Smith, S. C. Solomon, D. O. Muhleman, J. W. Head, J. B. Garvin, J. B. Abshire, and J. L. Bufton (1992), Mars Observer Laser Altimeter investigation, *J. Geophys. Res.*, *97*, 7781–7798.

R. E. Arvidson, Department of Earth and Planetary Sciences, Washington University, St. Louis, MO 63130, USA.

A. Gendrin, Department of Geological Sciences, Brown University, Providence, RI 02912, USA.

J. L. Griffes, Center for Earth and Planetary Studies, National Air and Space Museum, Smithsonian Institution, Independence Avenue at 6th Street SW, Washington, DC 20013, USA. (griffesj@si.edu)

F. Poulet, Institut d'Astrophysique Spatiale, Université Paris-Sud, Orsay Cedex, F-91405, France.